
Overcoming the Paradox of Certified Training with Gaussian Smoothing

Stefan Balaucă^{1*} Mark Niklas Müller² Yuhao Mao²
 Maximilian Baader² Marc Fischer² Martin Vechev²

¹ INSAIT, Sofia University, Bulgaria ² ETH Zurich, Switzerland

Abstract

Training neural networks with high certified accuracy against adversarial examples remains an open problem despite significant efforts. While certification methods can effectively leverage tight convex relaxations for bound computation, in training, these methods perform worse than looser relaxations. Prior work hypothesized that this is caused by the discontinuity and perturbation sensitivity of the loss surface induced by these tighter relaxations. In this work, we show theoretically that Gaussian Loss Smoothing can alleviate both issues. We confirm this empirically by proposing a certified training method combining PGPE, an algorithm computing gradients of a smoothed loss, with different convex relaxations. When using this training method, we observe that tighter bounds indeed lead to strictly better networks. While scaling PGPE training remains challenging due to high computational cost, we show that by using a not theoretically sound, yet much cheaper smoothing approximation, we obtain better certified accuracies than state-of-the-art methods when training on the same network architecture. Our results clearly demonstrate the promise of Gaussian Loss Smoothing for training certifiably robust neural networks.

1 Introduction

The increased deployment of deep learning systems in mission-critical applications has made their provable trustworthiness and robustness against adversarial examples (Biggio et al., 2013; Szegedy et al., 2014) an important topic. As state-of-the-art neural network certification has converged to similar approaches (Zhang et al., 2022; Ferrari et al., 2022), increasingly reducing the verification gap, the focus in the field is now shifting to specialized training methods that yield networks with high certified robustness while minimizing the loss of standard accuracy (Müller et al., 2023; De Palma et al., 2023).

Certified Training State-of-the-art certified training methods aim to optimize the network’s worst-case loss over an input region defined by an adversarial specification. However, as computing the exact worst-case loss is NP-complete (Katz et al., 2017), they typically utilize convex relaxations to compute over-approximations (Gowal et al., 2018; Singh et al., 2018, 2019). Surprisingly, training methods based on the least precise relaxations (IBP) empirically yield the best performance (Shi et al., 2021), while tighter relaxations perform progressively worse (left, Figure 1). Jovanović et al. (2022) investigated this surprising phenomenon which they call the “Paradox of Certified Training”, both theoretically and empirically and found that tighter relaxations induce harder optimization problems. Specifically, they identify the *continuity* and *sensitivity* of the loss surface induced by a relaxation as key factors for the success of certified training, beyond its *tightness*. Indeed, *all* state-of-the-art

*Correspondence to stefan.balaucă@insait.ai

methods are based on the imprecise but continuous and insensitive IBP bounds (Müller et al., 2023; Mao et al., 2023a; De Palma et al., 2023). However, while these IBP-based methods improve robustness, they induce severe regularization, significantly limiting the effective capacity and thus standard accuracy (Mao et al., 2023b). Overall, this raises the following fundamental question:

Can the paradox of certified training and thus the robustness-accuracy trade-off be overcome?

This Work: Overcoming the Paradox In this work we propose a conceptual path forward to overcoming the paradox. Concretely, we introduce the first certified training method based on gradient-free optimization which smooths the discontinuity and sensitivity of the loss surface. Our method leverages *Gaussian Loss Smoothing*, inducing both continuity and infinite differentiability by smoothing the worst-case loss approximation with a Gaussian kernel. Specifically, we propose the first backpropagation-free certified training method, recovering Gaussian Loss Smoothing in expectation. Our approach is based on PGPE (Sehnke et al., 2010), which in the context of neuro-evolutionary algorithms was recently shown to be one of the best performing for supervised learning (Lange et al., 2023). Using this method, we empirically demonstrate that tighter relaxations now lead to strictly better networks, thereby confirming the importance of continuity and sensitivity in the paradox of certified training and overcoming it (right, Figure 1). With PGPE, we also show that the more precise DEEPOLY relaxation (Singh et al., 2019) achieves strictly better results than the less precise IBP. Moreover, we demonstrate that the advantages of Gaussian Loss Smoothing combined with DEEPOLY improve with increasing network depth, outperforming state-of-the-art methods applied on the same architecture. Further, to mitigate the high computational cost of PGPE, we propose an approximation of Gaussian Loss Smoothing based on Randomized Gradient Smoothing, leveraging recent advancements Starnes et al. (2023). This approximation retains the strong performance of Gaussian Loss Smoothing with up to 40x speedups.

Main Contributions Our core contributions are:

- (1) A theoretical investigation on how Gaussian Loss Smoothing affects both continuity and sensitivity of the approximate worst-case loss in certified training.
- (2) A novel PGPE-based certified training method that leverages the above insights and achieves the tightness of DeepPoly bounds while ensuring continuity via Gaussian Loss Smoothing.
- (3) A comprehensive empirical evaluation of different convex relaxations under PGPE optimization, requiring over 100,000 GPU hours, and demonstrating the promise of Loss Smoothing based approaches.
- (4) An approximation of Gaussian Loss Smoothing based on Randomized Gradient Smoothing, achieving up to 40x speedup compared to PGPE while maintaining strong performance.

We believe our work demonstrates the promise of Gaussian Loss Smoothing for certified training, suggesting interesting and fruitful directions for future work, including further scaling the presented methods, novel techniques to smooth the certified loss, and other combinations of gradient-based and gradient-free training.

2 Training for Certified Robustness

Below, we first introduce our notation and the setting of adversarial robustness before providing a background on (training for) certified robustness.

Notation We denote vectors with bold lower-case letters $\mathbf{a} \in \mathbb{R}^n$, matrices with bold upper-case letters $\mathbf{A} \in \mathbb{R}^{n \times d}$, and sets with upper-case calligraphic letters $\mathcal{A} \subset \mathbb{R}$. All inequalities $\mathbf{a} \geq \mathbf{b}$ between vectors hold elementwise.

Relaxation	Tightness	GRAD	PGPE
IBP	0.55	91.23	87.02
CROWN-IBP	1.68	88.76	90.23
DEEPOLY	2.93	90.04	91.53

Figure 1: Illustration of how Gaussian loss smoothing overcomes the paradox of certified training. We compare the certified accuracy [%] obtained by training with different relaxations using either the standard gradient (GRAD) or a gradient estimate computed on the smoothed loss surface (PGPE) with the tightness of the method.

2.1 Adversarial Robustness

We consider a neural network $\mathbf{f}_\theta(\mathbf{x}): \mathcal{X} \rightarrow \mathbb{R}^n$, parameterized by the weights θ , that assigns a score to each class $i \in \mathcal{Y}$ given an input $\mathbf{x} \in \mathcal{X}$. This induces the classifier $F: \mathcal{X} \rightarrow \mathcal{Y}$ as $F(\mathbf{x}) := \arg \max_i \mathbf{f}_\theta(\mathbf{x})_i$. We call F locally robust for an input $\mathbf{x} \in \mathcal{X}$ if it predicts the same class $y \in \mathcal{Y}$ for all inputs in an ϵ -neighborhood $\mathcal{B}_p^\epsilon(\mathbf{x}) := \{\mathbf{x}' \in \mathcal{X} \mid \|\mathbf{x} - \mathbf{x}'\|_p \leq \epsilon\}$. To prove that a classifier is locally robust, we thus have to show that $F(\mathbf{x}') = F(\mathbf{x}) = y, \forall \mathbf{x}' \in \mathcal{B}_p^\epsilon(\mathbf{x})$.

Local robustness is equivalent to the log-probability of the target class y being greater than that of all other classes for all relevant inputs, i.e., $\min_{\mathbf{x}' \in \mathcal{B}, i \neq y} f(\mathbf{x}')_y - f(\mathbf{x})_i > 0$. As solving this neural network verification problem exactly is generally NP-complete (Katz et al., 2017), state-of-the-art neural network verifiers relax it to an efficiently solvable convex optimization problem (Brix et al., 2023). To this end, the non-linear activation functions are replaced with convex relaxations in their input-output space, allowing linear bounds of the following form on their output $f(\mathbf{x})$ to be computed:

$$\mathbf{A}_l \mathbf{x} + \mathbf{b}_l \leq \mathbf{f}_\theta(\mathbf{x}) \leq \mathbf{A}_u \mathbf{x} + \mathbf{b}_u,$$

for some input region $\mathcal{B}_p^\epsilon(\mathbf{x})$. These bounds can in-turn be bounded concretely by $\mathbf{l}_y = \min_{\mathbf{x} \in \mathcal{B}} \mathbf{A}_{l_i} \mathbf{x} + \mathbf{b}_{l_i} \in \mathbb{R}$ and \mathbf{u}_y analogously. Hence, we have $\mathbf{l}_y \leq \mathbf{f}(\mathbf{x}) \leq \mathbf{u}_y$.

Training for Robustness To obtain (certifiably) robust neural networks, specialized training methods are required. For a data distribution $(\mathbf{x}, t) \sim \mathcal{D}$, standard training optimizes the network parametrization θ to minimize the expected cross-entropy loss:

$$\theta_{\text{std}} = \arg \min_{\theta} \mathbb{E}_{\mathcal{D}} [\mathcal{L}_{\text{CE}}(\mathbf{f}_\theta(\mathbf{x}), t)], \quad \text{with} \quad (1)$$

$$\mathcal{L}_{\text{CE}}(\mathbf{y}, t) = \ln \left(1 + \sum_{i \neq t} \exp(y_i - y_t) \right). \quad (2)$$

To train for robustness, we, instead, aim to minimize the expected *worst-case loss* for a given robustness specification, leading to a min-max optimization problem:

$$\theta_{\text{rob}} = \arg \min_{\theta} \mathbb{E}_{\mathcal{D}} \left[\max_{\mathbf{x}' \in \mathcal{B}^\epsilon(\mathbf{x})} \mathcal{L}_{\text{CE}}(\mathbf{f}_\theta(\mathbf{x}'), t) \right]. \quad (3)$$

As computing the worst-case loss by solving the inner maximization problem is generally intractable, it is commonly under- or over-approximated, yielding adversarial and certified training, respectively.

Adversarial Training optimizes a lower bound on the inner optimization objective in Equation (3). To this end, it first computes concrete examples $\mathbf{x}' \in \mathcal{B}^\epsilon(\mathbf{x})$ that approximately maximize the loss term \mathcal{L}_{CE} and then optimizes the network parameters θ for these examples. While networks trained this way typically exhibit good empirical robustness, they remain hard to formally certify and are sometimes vulnerable to stronger attacks (Tramèr et al., 2020; Croce and Hein, 2020).

Certified Training typically optimizes an upper bound on the inner maximization objective in Equation (3). To this end, the robust cross-entropy loss $\mathcal{L}_{\text{CE,rob}}(\mathcal{B}^\epsilon(\mathbf{x}), t) = \mathcal{L}_{\text{CE}}(\bar{\mathbf{y}}^\Delta, t)$ is computed from an upper bound $\bar{\mathbf{y}}^\Delta$ on the logit differences $\mathbf{y}^\Delta := \mathbf{y} - \mathbf{y}_t$ obtained via convex relaxations as described above and then plugged into the standard cross-entropy loss.

As this can induce strong over-regularization if the used convex relaxations are imprecise and thereby severely reduce the standard accuracy of the resulting models, current state-of-the-art certified training methods combine these bounds with adversarial training (De Palma et al., 2022; Müller et al., 2023; Mao et al., 2023a; De Palma et al., 2023). We now introduce the convex relaxations popular for neural networks.

2.2 Convex Relaxations

We now discuss four popular convex relaxations of different precision, investigated in this work.

IBP Interval bound propagation (Mirman et al., 2018; Gehr et al., 2018; Gowal et al., 2018) only considers elementwise, constant bounds of the form $\mathbf{l} \leq \mathbf{v} \leq \mathbf{u}$. Affine layers $\mathbf{y} = \mathbf{W}\mathbf{v} + \mathbf{b}$ are thus also relaxed as

$$\frac{\mathbf{W}(\mathbf{l}+\mathbf{u}) - |\mathbf{W}|(\mathbf{u}-\mathbf{l})}{2} + \mathbf{b} \leq \mathbf{W}\mathbf{v} + \mathbf{b} \leq \frac{\mathbf{W}(\mathbf{l}+\mathbf{u}) + |\mathbf{W}|(\mathbf{u}-\mathbf{l})}{2} + \mathbf{b},$$

where $|\cdot|$ is the elementwise absolute value. ReLU functions are relaxed by their concrete lower and upper bounds $\text{ReLU}(\mathbf{l}) \leq \text{ReLU}(\mathbf{v}) \leq \text{ReLU}(\mathbf{u})$, illustrated in Figure 2a.

Hybrid Box (HBox) The HBox relaxation is an instance of Hybrid Zonotope (Mirman et al., 2018) which combines the exact encoding of affine transformations from the DEEPZ or Zonotope domain (Singh et al., 2018; Wong and Kolter, 2018; Weng et al., 2018; Wang et al., 2018) with the simple IBP relaxation of unstable ReLUs, illustrated in Figure 2a. While less precise than DEEPZ, HBOX ensures constant instead of linear representation size in the network depth, making its computation much more efficient.

DeepPoly DEEPPOLY, introduced by Singh et al. (2019), is mathematically identical to CROWN (Zhang et al., 2018) and based on recursively deriving linear bounds of the form

$$\mathbf{A}_l \mathbf{x} + \mathbf{a}_l \leq \mathbf{v} \leq \mathbf{A}_u \mathbf{x} + \mathbf{a}_u$$

on the outputs of every layer. While this handles affine layers exactly, ReLU layers $\mathbf{y} = \text{ReLU}(\mathbf{v})$ are relaxed neuron-wise, using one of the two relaxations illustrated in Figure 2b:

$$\lambda \mathbf{v} \leq \text{ReLU}(\mathbf{v}) \leq (\mathbf{v} - \mathbf{l}) \frac{\mathbf{u}}{\mathbf{u} - \mathbf{l}},$$

where product and division are elementwise. The lower-bound slope $\lambda = \mathbb{1}_{|u| > |l|}$ is chosen depending on the input bounds \mathbf{l} and \mathbf{u} to minimize the area between the upper- and lower-bound in the input-output space. Crucially, a minor change in the input bounds can thus lead to a large change in output bounds when using the DEEPPOLY relaxation.

CROWN-IBP To reduce the computational complexity of DEEPPOLY, CROWN-IBP (Zhang et al., 2020) uses the cheaper but less precise IBP bounds to compute the concrete upper- and lower-bounds \mathbf{u} and \mathbf{l} on ReLU inputs required for the DEEPPOLY relaxation. To compute the final bounds on the network output DEEPPOLY is used. This reduces the computational complexity from quadratic to linear in the network depth. While, CROWN-IBP is not strictly more or less precise than either IBP or DEEPPOLY, its precision empirically lies between the two.

Relaxation Tightness While we rarely have strict orders in tightness (only HBOX is strictly tighter than IBP), we can compare the tightness of relaxations empirically given a network to analyze. Jovanović et al. (2022) propose to measure the tightness of a relaxation as the AUC score of its certified accuracy over perturbation radius curve. This metric implies the following empirical tightness ordering $\text{IBP} < \text{HBox} < \text{CROWN-IBP} < \text{DEEPPOLY}$ (Jovanović et al., 2022), which agrees well with our intuition.

2.3 The Paradox of Certified Training

For networks, certified with convex relaxations, higher robustness is achieved by sacrificing standard accuracy. Usually, more precise relaxations induce less overapproximation and thus less regularization, potentially leading to better standard and certified accuracy. However, empirically the least precise relaxation, IBP, dominates the more precise methods, e.g., DEEPPOLY, with respect to both certified and standard accuracy (see the left-hand side of Figure 1). This is all the more surprising given that state-of-the-art certified training methods introduce artificial unsoundness into these IBP bounds to improve tightness at the cost of soundness to reduce regularization and improve performance (Müller et al., 2023; Mao et al., 2023a; De Palma et al., 2023).

Jovanović et al. (2022) explained this paradox, by showing that these more precise relaxations induce loss landscapes suffering from discontinuities and high sensitivity, making it extraordinarily challenging for gradient-based optimization methods to find good optima. Thus the key challenge of certified training is to design a robust loss that combines tight bounds with a continuous and smooth loss landscape. Next, we discuss these challenges in more detail and show how to overcome them.

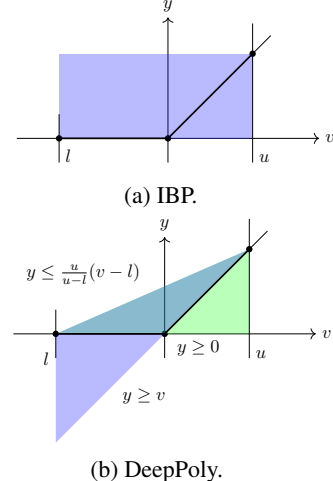


Figure 2: IBP (left) and DEEPPOLY (right) relaxations of a ReLU with bounded inputs $v \in [l, u]$. For DEEPPOLY the lower-bound slope λ is chosen to minimize the area between the upper- and lower-bound in the input output space, resulting in the blue or green area.

3 Gaussian Loss Smoothing (GLS) for Certified Training

In this section, we first discuss Gaussian Loss Smoothing in policy gradient methods before showing how they can be applied to certified training. We defer the proofs to App. B.

3.1 Policy Gradients with Parameter-based Exploration

PGPE (Sehnke et al., 2010) is a gradient-free optimization algorithm that optimizes the Gaussian Smoothing loss $L_\sigma(\theta) := \mathbb{E}_{\theta' \sim \mathcal{N}(\theta, \sigma^2 I)} \hat{L}(f_{\theta'})$, where the loss is not evaluated at a single parameterization of the network, but rather at a (normal) distribution of parameterizations.

PGPE samples weight perturbation $\epsilon_i \sim \mathcal{N}(0, \sigma^2)$, and evaluates the loss on $\theta + \epsilon_i$, and $\theta - \epsilon_i$, computing $r_i^+ = L(\theta + \epsilon_i)$ and $r_i^- = L(\theta - \epsilon_i)$. These pairs of symmetric points are then used to compute gradient estimates with respect to both the mean of the weight distribution θ and its standard deviation σ :

$$\begin{aligned}\nabla_\theta \hat{L}_\sigma(\theta) &\propto \sum_i \epsilon_i (r_i^+ - r_i^-), \\ \nabla_\sigma \hat{L}_\sigma(\theta) &\propto \sum_i \left(\frac{r_i^+ + r_i^-}{2} - b \right) \frac{\epsilon_i^2 - \sigma_i^2}{\sigma_i},\end{aligned}$$

where $b = \frac{1}{2n} \sum_i r_i^+ + r_i^-$ is called baseline loss and is the loss mean over all $2n$ samples. Figure 3 visualizes such a gradient estimate. Both gradient approximations $\nabla_\theta \hat{L}_\sigma(\theta)$ and $\nabla_\sigma \hat{L}_\sigma(\theta)$ are used to update the mean weights θ and the standard deviation σ , respectively.

By design, PGPE recovers an unbiased estimate of the gradients on the Gaussian smoothed loss, see:

Lemma 3.1. *PGPE approximately minimizes the smoothed loss $L_\sigma(\theta)$ by sampling. In particular, the expectation of the PGPE update on θ is the true gradient of $L_\sigma(\theta)$, i.e., $\mathbb{E} \nabla_\theta \hat{L}_\sigma(\theta) = \nabla_\theta L_\sigma(\theta)$.*

As no backward propagation is needed to compute these gradient estimates, PGPE is comparable to neuro-evolution algorithms. In this context it is among the best performing methods for supervised learning (Lange et al., 2023).

3.2 Open Challenges: Discontinuity and Sensitivity

Recall §2.3, where we discussed the key challenges of certified training with tighter relaxations, namely discontinuity and sensitivity of the loss surface. We illustrate these key challenges on a toy network and loss in Figure 4.

On the left-hand side (Original in Figure 4a), we show the DEEPOLY lower bound of the one-neuron network $y = \text{ReLU}(x + w) + 1$ for $x \in [-1, 1]$ over the parameter w . As the original bound $l = 1 + \mathbb{1}_{w>0} \cdot (w - 1)$ is discontinuous at $w = 0$, a gradient-based optimization method initialized at $w > 0$ will decrease w until it has moved through the discontinuity and past the local minimum.

The second key factor, sensitivity, can be interpreted as a combination of the number of local minima and the smoothness of the loss-landscape. Jovanović et al. (2022) show that DEEPOLY is more sensitive than IBP, making it more likely that gradient-based optimization methods will get stuck in bad local minima. We illustrate this with the toy function shown in Figure 4b. Here the original function has a bad local minimum for $w \in [-1.5, 0]$ that a gradient-based optimizer can get stuck in.

We now discuss how Gaussian Loss Smoothing can address both of these challenges.

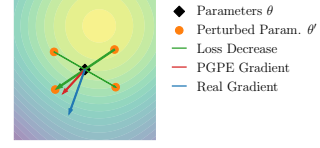


Figure 3: Illustration the PGPE algorithm: First we sample random perturbations around the central point θ from a Gaussian distribution with standard deviation σ . Then we compute the loss difference between pairs of symmetric points. Finally, we estimate the gradient as a sum of sampled directions weighted by the magnitude of loss change in each direction.

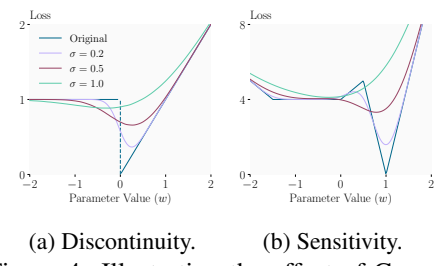


Figure 4: Illustrating the effect of Gaussian Loss Smoothing on the discontinuity (left) and sensitivity of loss functions (right).

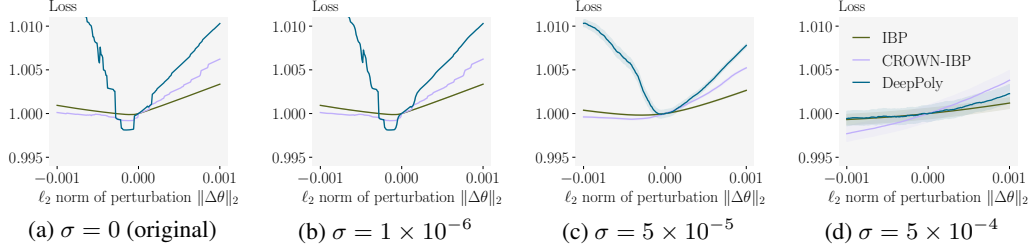


Figure 5: The original and Gaussian smoothed loss for different relaxations on a PGD-trained CNN3, evaluated along the direction of DEEPOLY gradient. Losses are normalized by dividing them with the values at 0, i.e., without perturbation. The smoothed loss is estimated with 128 samples and the corresponding confidence interval is shown as shaded.

3.3 Gaussian Loss Smoothing for Certified Training

First, Gaussian Loss Smoothing (GLS) turns any discontinuous loss function (such as the one in Figure 4a) into a continuous one that is differentiable everywhere. More formally:

Corollary 3.2. *The loss surface under GLS is continuous, infinitely differentiable for any reasonably growing loss function $L(\theta)$.*

Second, Gaussian Smoothing can help to overcome the sensitivity issue. As we show in Figure 4b, depending on the standard deviation, the local minimum can be reduced or removed, and the loss landscape can be smoothed. However, the choice of standard deviation is crucial. While a too small standard deviation only has a minimal effect on loss smoothness and might not remove local minima, a too large standard deviation can oversmooth the loss, completely removing or misaligning minima. We again illustrate this in Figure 4b. There, a small standard deviation of $\sigma = 0.2$ does not smooth out the local minimum while a large standard deviation ($\sigma = 1.0$) severely misaligns the new global minimum with that of the original function. We can formalize this result as proven by Sehnke et al. (2010), based on the notion of β -smoothness (a function f is β -smooth if its gradient is β -Lipschitz-continuous, i.e. $\|\nabla f(x) - \nabla f(x')\| < \beta\|x - x'\|$ for some real constant β):

Corollary 3.3. *The loss surface under GLS is β_1 -smooth for any reasonably growing β_2 -smooth loss function $L(\theta)$. The bounding constant β_1 of the GLS loss gradient is also less than or equal to the bounding constant β_2 of the original loss gradient.*

Hence, GLS has the potential to mitigate the key issues, discontinuity and sensitivity, for tight convex relaxations (as identified by Jovanović et al. (2022)).

Empirical Confirmation To empirically confirm these effects, we plot the original and smoothed loss landscape (along the direction of the DEEPOLY gradient) of different relaxations for a CNN3 and different standard deviations in Figure 5. We normalize all losses by dividing them by their value for the unperturbed weights.

We observe that the original loss (Figure 5a) is discontinuous and highly sensitive to perturbations for both CROWN-IBP and DEEPOLY, consistent with the findings of Jovanović et al. (2022). Only the imprecise IBP loss is continuous and smooth, explaining why the IBP loss is the basis for many successful certified training methods. When the loss is smoothed with small standard deviations $\sigma = 10^{-6}$ (Figure 5b), the local minimum of the DEEPOLY loss has a slightly reduced sharpness but is still present. In addition, both the losses for DEEPOLY and CROWN-IBP are still highly sensitive. This indicates a too small σ .

When the standard deviation is increased to $\sigma = 5 \cdot 10^{-5}$ (Figure 5c), the undesirable local minimum of the DEEPOLY loss is removed completely, and both losses become much less sensitive to perturbations. However, further increasing the standard deviation to $\sigma = 5 \cdot 10^{-4}$ (Figure 5d), leads to almost flat losses removing the minimum present in the underlying loss.

These results empirically confirm the observations in our toy setting and predicted by our theoretical analysis, showing that Gaussian Loss Smoothing (via PGPE) mitigates the discontinuity and sensitivity issues formulated by Jovanović et al. (2022).

3.4 Approximating Gaussian Loss Smoothing via Random Gradient Smoothing

While the Loss Smoothing induced by the sampling procedure of PGPE leads to a provably continuous and infinitely differentiable loss surfaces, it can be costly to compute. To reduce the computational cost, we propose to approximate GLS by Randomized Gradient Smoothing (Duchi et al., 2012). RGS approximates the gradient of the smoothed loss by sampling points $\theta + \epsilon_i$ and then averaging the gradients at these perturbed points:

$$\nabla_{\theta} \hat{L}_{\sigma}(\theta) \propto \frac{1}{n} \sum_i \nabla_{\theta} L_{\sigma}(\theta + \epsilon_i).$$

While RGS does not provably recover in expectation the gradient of the smoothed loss, (see App. B.3 for more details), Duchi et al. (2012) have shown its empirical effectiveness, even with a tiny sample size ($n = 2$). Therefore, we apply this alternative to study the performance of GLS in larger networks. Further, contrary to before, σ is now a hyperparameter that needs to be tuned. We decay σ during training to improve convergence. A comparison of training costs is included in App. E.6, where RGS is up to 40 times faster than PGPE.

Encouraged by these results, we next empirically evaluate the performance of PGPE- and RGS-based certified training methods.

4 Experimental Evaluation

In this section, we rigorously evaluate the effect of Gaussian Loss Smoothing via PGPE on the training characteristics of different bound computation methods.

First, we show in §4.1 that the ‘‘Paradox of Certified Training’’ (Jovanović et al., 2022) can be overcome by smoothing the loss surface, i.e., that under Gaussian Loss Smoothing, training with tighter bounds will generally lead to better certified and standard accuracy. Second, we show in §4.2 that the effects outlined above become even more pronounced as we scale to deeper networks. Further, we investigate how the hyperparameters of PGPE affect the properties of the induced loss surface and thus interact with the performance of the resulting certified training method in App. C.

Experimental Setup We implement all certified training methods in PyTorch (Paszke et al., 2019) and conduct experiments on MNIST (LeCun et al., 2010) and CIFAR-10 (Krizhevsky et al., 2009) using l_{∞} perturbations and modified versions of the CNN3 and CNN5 architectures (see Table 5 in App. E). For more details on the experimental setting including all hyperparameters, see App. E.

Standard Certified Training For standard certified training using back-propagation (referred to below as GRAD for clarity), we use similar hyperparameters as recent work in the space (Shi et al., 2021; Müller et al., 2023; Mao et al., 2023a; De Palma et al., 2023) and initialize all models using the IBP initialization proposed by Shi et al. (2021). In particular, we also use the Adam optimizer (Kingma and Ba, 2015), follow their learning rate and ϵ -annealing schedule, use the same batch size and gradient clipping threshold, and use the same ϵ for training and certification. In the case of SABR, STAPS and MTL-IBP, we conduct an extensive optimization of their network-specific hyperparameters and only report the best one.

PGPE Training We train our PGPE models using the multi-GPU, multi-actor implementation from evotorch (Toklu et al., 2023). As PGPE training is computationally expensive, we initialize from a PGD-trained model. This can be seen as a warm-up stage as is common also for other certified training methods (Shi et al., 2021; Müller et al., 2023; Mao et al., 2023a). We only use ϵ -annealing for the larger perturbation magnitudes on both MNIST and CIFAR-10 and choose learning-rate schedules based on a brief initial evaluation of training stability. Unless indicated otherwise, we run the PGPE algorithm with a population size of $n_{ps} = 256$ and an initial standard deviation for weight sampling of $\sigma_{\text{PGPE}} = 10^{-3}$.

RGS Training We train our RGS models using the same hyperparameters as for PGPE training, but with a population size of $n_{ps} = 2$ and shorter schedules to reduce costs. As RGS does not dynamically adjust the standard deviation, we choose to decay it at the same time steps as the learning rate. More details for the hyperparameters used can be found in App. E.

Table 1: Comparison of the standard (Acc.) and certified (Cert. Acc.) accuracy of CNN3 network trained with different certified training methods on the full MNIST and CIFAR-10. We use the state-of-the-art method MN-BAB (Ferrari et al., 2022) for certification.

Dataset	ϵ_∞	Relaxation	Nat. Acc. [%]		Cert. Acc. [%]		Adv. Acc. [%]	
			GRAD	PGPE	GRAD	PGPE	GRAD	PGPE
MNIST	0.1	PGD	98.43	-	87.27	-	91.62	-
		IBP	96.02	94.52	91.23	87.02	91.23	87.03
		HBOX	94.79	96.12	88.18	90.57	88.18	90.58
		CROWN-IBP	94.33	96.69	88.76	90.23	88.77	90.25
		DEEPPOLY	95.95	97.44	90.04	91.53	90.08	91.79
	0.3	PGD	96.08	-	75.14	-	77.44	-
		IBP	91.02	89.16	77.23	74.00	77.27	74.08
		HBOX	83.75	86.58	57.86	70.52	57.92	70.66
		CROWN-IBP	86.97	90.57	70.55	71.95	70.56	72.24
		DEEPPOLY	85.70	91.05	66.69	74.28	66.70	74.98
CIFAR 10	2/255	PGD	60.35	-	34.62	-	40.12	-
		IBP	48.05	44.55	37.69	34.09	37.70	34.10
		CROWN-IBP	44.49	51.19	35.75	37.51	35.75	37.65
		DEEPPOLY	47.70	54.17	36.72	38.95	36.72	40.20
	8/255	PGD	50.18	-	7.90	-	19.65	-
		IBP	34.63	30.48	25.72	21.75	25.74	21.75
		CROWN-IBP	31.60	32.36	22.66	21.40	22.66	21.42
		DEEPPOLY	33.06	31.37	22.97	22.19	22.98	22.19

Certification We use the state-of-the-art complete verification method MN-BAB (Ferrari et al., 2022) with the same settings as used by Müller et al. (2023) for all networks independently of the training method. We note that this is in contrast to Jovanović et al. (2022) who used the same method for training and verification. However, we aim to assess true robustness instead of certifiability with the same bounding method used during training.

Hardware For PGPE and RGS training, we used between 2 and 8 NVIDIA L4-24GB GPUs. For standard certified training and certification, we used single L4 GPUs. See App. E.6 for a detailed breakdown of the computational cost.

4.1 Overcoming the Paradox of Certified Training

In Table 1, we compare the performance of training with various convex relaxations using either standard backpropagation (GRAD) or the Gaussian loss smoothing (PGPE).

GRAD Training We train the same CNN3 on MNIST and CIFAR-10 at the established perturbation magnitudes using standard certified training with IBP, HBOX, CROWN-IBP, and DEEPPOLY. We observe that across all these settings IBP dominates the other methods both in terms of standard and certified accuracy, confirming the paradox of certified training. Specifically, HBOX, CROWN-IBP, and DEEPPOLY tend to perform similarly, with CROWN-IBP being significantly better at MNIST $\epsilon = 0.3$, indicating that in the absence of continuity and for high sensitivity, tightness is less relevant.

PGPE Training Training the same CNN3 in the same settings with PGPE we observe that the performance ranking changes significantly (see Table 1). Now, training with IBP performs strictly worse than training with DEEPPOLY across all datasets and perturbation sizes. In fact, the more precise DEEPPOLY bounds now yield the best certified accuracy across all settings, even outperforming GRAD-based training methods at low perturbation radii. Interestingly IBP still yields better certified accuracy at large perturbation radii than HBOX and CROWN-IBP, although at significantly worse natural accuracies. This is likely because more severe regularization is required in these settings.

This shows that PGPE indeed mitigates the sensitivity and discontinuity issues of more precise convex relaxations, by leveraging Gaussian Loss Smoothing. As PGPE does not require differentiability, this points to future training methods based on even more precise bounds than DEEPPOLY, computed, e.g., via a branch and bound-based procedure or multi-neuron constraints.

While DEEPPOLY + PGPE outperforms DEEPPOLY + GRAD in almost all settings in Table 1 on the same network architecture, sometimes by a wide margin, it does not reach the general SOTA results of classic and heavily optimized GRAD training methods. We believe this is caused by three key factors: First, PGPE computes a gradient approximation in an $\frac{n_{ps}}{2}$ -dimensional subspace. To cover the full parameter space, we would need the population size n_{ps} to be twice the number of

network parameters, which is computationally intractable even for small networks. Thus, we only get low-dimensional gradient approximates, slowing down training (see Table 3 and Figure 7). Second, again due to the high cost of training with PGPE, we used relatively short training schedules and were unable to optimize hyperparameters for the different settings. Finally, PGPE-based certified training is less optimized, compared to standard certified training which has been extensively optimized over the past years (Shi et al., 2021; Müller et al., 2023; De Palma et al., 2023).

4.2 Scaling to Deeper Networks with Randomized Gradient Smoothing

Previously, we demonstrated the theoretical and empirical advantages of GLS instantiated with PGPE. However, PGPE is computationally intractable except for very small networks, more scalable methods are required. In this section, we investigate one such method, namely Randomized Gradient Smoothing (RGS), as defined in §3.4. We show that RGS achieves strong empirical performance while being much more scalable, even though RGS does not fully resolve the discontinuity issue (see App. B.3).

While RGS cannot always recover in expectation the gradient of the smoothed loss surface, it overcomes the low-rank gradient and computational cost issues of PGPE: even with a small population size (hence low training costs) we obtain full-rank gradient approximations, enabling faster and better optimization. We analyze the results of training with RGS on the CNN5 architecture in Table 2. Encouragingly, RGS significantly boosts the performance of DEEPPOLY training. We observe that DEEPPOLY + RGS dominates all other methods, substantially improving even over state-of-the-art GRAD-based methods with hyperparameters fine-tuned on CNN5. Further, the performance of DEEPPOLY + RGS on the small CNN5 becomes comparable to the performance of GRAD-IBP on the deeper and 4 times wider CNN7 architecture used by most recent state-of-the-art methods (De Palma et al., 2023), without batch norm layers and special training tricks designed for IBP (Shi et al., 2021). This result agrees well with our expectation that bound tightness becomes increasingly important with network depth, as errors can grow exponentially with depth (Shi et al., 2021; Müller et al., 2023; Mao et al., 2023b).

5 Limitations

Training with PGPE in combination with DEEPPOLY is computationally expensive, preventing experiments with larger architectures. Despite these computational limitations, the method does propose a novel research direction for overcoming the certified training paradox. To address the scaling challenge, we believe that future investigations should focus on more computationally efficient smoothing approaches for certified training. As a step in this direction, we propose RGS, a much more scalable alternative to PGPE, one that drastically improves scalability.

6 Conclusion

In this work, we showed that the paradox of certified training, i.e., that tighter relaxations perform worse for certified training, can be overcome by inducing a smooth loss surface. Specifically, for certified training, we instantiated Gaussian Loss Smoothing with PGPE and demonstrated that tighter bounds lead to networks with strictly better performance. Further, as PGPE is computationally costly, we proposed Randomized Gradient Smoothing as an approximation of Gaussian Loss Smoothing. RGS achieves better certified accuracies than state-of-the-art methods on the same network architecture. While RGS is still computationally costly, it highlights a promising direction for future work and confirms the crucial importance of loss continuity and sensitivity in certified training.

Table 2: Accuracies of a CNN5 depending on training method.

Dataset	ϵ_∞	Method	Nat	Cert	Adv
MNIST	0.1	IBP	97.94	95.82	95.83
		SABR	98.81	96.28	96.31
		STAPS	98.74	96.05	96.09
		MTL-IBP	98.74	96.25	96.29
		DEEPPOLY	98.50	95.95	95.97
		DEEPPOLY-RGS	99.34	97.56	97.70
		<i>IBP-CNN7</i>	99.15	98.02	98.08
CIFAR-10	2/255	IBP	54.92	45.36	45.36
		SABR	66.73	52.11	52.55
		MTL-IBP	67.03	53.81	55.18
		DEEPPOLY	65.43	53.16	54.10
		DEEPPOLY-RGS	67.62	54.83	56.05
		<i>IBP-CNN7</i>	66.10	55.04	55.22

Acknowledgements

This work has been done as part of the EU grant ELSA (European Lighthouse on Secure and Safe AI, grant agreement no. 101070617) and the SERI grant SAFEAI (Certified Safe, Fair and Robust Artificial Intelligence, contract no. MB22.00088). Views and opinions expressed are however those of the authors only and do not necessarily reflect those of the European Union or European Commission. Neither the European Union nor the European Commission can be held responsible for them.

The work has received funding from the Swiss State Secretariat for Education, Research and Innovation (SERI).

This research was partially funded by the Ministry of Education and Science of Bulgaria (support for INSAIT, part of the Bulgarian National Roadmap for Research Infrastructure).

References

B. Biggio, I. Corona, D. Maiorca, B. Nelson, N. Srndic, P. Laskov, G. Giacinto, and F. Roli, “Evasion attacks against machine learning at test time,” in *Proc of ECML PKDD*, 2013.

C. Szegedy, W. Zaremba, I. Sutskever, J. Bruna, D. Erhan, I. J. Goodfellow, and R. Fergus, “Intriguing properties of neural networks,” in *Proc. of ICLR*, 2014.

H. Zhang, S. Wang, K. Xu, L. Li, B. Li, S. Jana, C. Hsieh, and J. Z. Kolter, “General cutting planes for bound-propagation-based neural network verification,” *ArXiv preprint*, vol. abs/2208.05740, 2022.

C. Ferrari, M. N. Müller, N. Jovanović, and M. T. Vechev, “Complete verification via multi-neuron relaxation guided branch-and-bound,” in *Proc. of ICLR*, 2022.

M. N. Müller, F. Eckert, M. Fischer, and M. T. Vechev, “Certified training: Small boxes are all you need,” in *Proc. of ICLR*, 2023.

A. De Palma, R. Bunel, K. Dvijotham, M. P. Kumar, R. Stanforth, and A. Lomuscio, “Expressive losses for verified robustness via convex combinations,” *CoRR*, vol. abs/2305.13991, 2023.

G. Katz, C. W. Barrett, D. L. Dill, K. Julian, and M. J. Kochenderfer, “Reluplex: An efficient SMT solver for verifying deep neural networks,” *ArXiv preprint*, vol. abs/1702.01135, 2017.

S. Gowal, K. Dvijotham, R. Stanforth, R. Bunel, C. Qin, J. Uesato, R. Arandjelovic, T. A. Mann, and P. Kohli, “On the effectiveness of interval bound propagation for training verifiably robust models,” *ArXiv preprint*, vol. abs/1810.12715, 2018.

G. Singh, T. Gehr, M. Mirman, M. Püschel, and M. T. Vechev, “Fast and effective robustness certification,” in *Proc. of NeurIPS*, 2018.

G. Singh, T. Gehr, M. Püschel, and M. T. Vechev, “An abstract domain for certifying neural networks,” *Proc. of POPL*, 2019.

Z. Shi, Y. Wang, H. Zhang, J. Yi, and C. Hsieh, “Fast certified robust training with short warmup,” in *Proc. of NeurIPS*, M. Ranzato, A. Beygelzimer, Y. N. Dauphin, P. Liang, and J. W. Vaughan, Eds., 2021.

N. Jovanović, M. Balunović, M. Baader, and M. T. Vechev, “On the paradox of certified training,” *Trans. Mach. Learn. Res.*, 2022.

Y. Mao, M. N. Mueller, M. Fischer, and M. Vechev, “Connecting certified and adversarial training,” in *Proc. of NeurIPS*, 2023.

Y. Mao, M. N. Müller, M. Fischer, and M. T. Vechev, “Understanding certified training with interval bound propagation,” *CoRR*, vol. abs/2306.10426, 2023.

F. Sehnke, C. Osendorfer, T. Rückstieß, A. Graves, J. Peters, and J. Schmidhuber, “Parameter-exploring policy gradients,” *Neural Networks*, 2010.

R. T. Lange, Y. Tang, and Y. Tian, “Neuroevobench: Benchmarking evolutionary optimizers for deep learning applications,” in *Proc. of NeurIPS Datasets and Benchmarks Track*, 2023.

A. Starnes, A. Dereventsov, and C. Webster, “Gaussian smoothing gradient descent for minimizing high-dimensional non-convex functions,” 2023.

C. Brix, M. N. Müller, S. Bak, T. T. Johnson, and C. Liu, “First three years of the international verification of neural networks competition (VNN-COMP),” *CoRR*, vol. abs/2301.05815, 2023.

F. Tramèr, N. Carlini, W. Brendel, and A. Madry, “On adaptive attacks to adversarial example defenses,” in *Proc. of NeurIPS*, 2020.

F. Croce and M. Hein, “Reliable evaluation of adversarial robustness with an ensemble of diverse parameter-free attacks,” in *Proc. of ICML*, 2020.

A. De Palma, R. Bunel, K. Dvijotham, M. P. Kumar, and R. Stanforth, “IBP regularization for verified adversarial robustness via branch-and-bound,” *ArXiv preprint*, vol. abs/2206.14772, 2022.

M. Mirman, T. Gehr, and M. T. Vechev, “Differentiable abstract interpretation for provably robust neural networks,” in *Proc. of ICML*, J. G. Dy and A. Krause, Eds., 2018.

T. Gehr, M. Mirman, D. Drachsler-Cohen, P. Tsankov, S. Chaudhuri, and M. T. Vechev, “AI2: safety and robustness certification of neural networks with abstract interpretation,” in *Proc. of S&P*, 2018.

E. Wong and J. Z. Kolter, “Provable defenses against adversarial examples via the convex outer adversarial polytope,” in *Proc. of ICML*, 2018.

T. Weng, H. Zhang, H. Chen, Z. Song, C. Hsieh, L. Daniel, D. S. Boning, and I. S. Dhillon, “Towards fast computation of certified robustness for relu networks,” in *Proc. of ICML*, 2018.

S. Wang, K. Pei, J. Whitehouse, J. Yang, and S. Jana, “Efficient formal safety analysis of neural networks,” in *Proc. of NeurIPS*, 2018.

H. Zhang, T. Weng, P. Chen, C. Hsieh, and L. Daniel, “Efficient neural network robustness certification with general activation functions,” in *Proc. of NeurIPS*, 2018.

H. Zhang, H. Chen, C. Xiao, S. Gowal, R. Stanforth, B. Li, D. S. Boning, and C. Hsieh, “Towards stable and efficient training of verifiably robust neural networks,” in *Proc. of ICLR*, 2020.

J. C. Duchi, P. L. Bartlett, and M. J. Wainwright, “Randomized smoothing for stochastic optimization,” 2012.

A. Paszke, S. Gross, F. Massa, A. Lerer, J. Bradbury, G. Chanan, T. Killeen, Z. Lin, N. Gimelshein, L. Antiga, A. Desmaison, A. Köpf, E. Yang, Z. DeVito, M. Raison, A. Tejani, S. Chilamkurthy, B. Steiner, L. Fang, J. Bai, and S. Chintala, “Pytorch: An imperative style, high-performance deep learning library,” in *Proc. of NeurIPS*, 2019.

Y. LeCun, C. Cortes, and C. Burges, “Mnist handwritten digit database,” *ATT Labs [Online]. Available: <http://yann.lecun.com/exdb/mnist>*, 2010.

A. Krizhevsky, G. Hinton *et al.*, “Learning multiple layers of features from tiny images,” 2009.

D. P. Kingma and J. Ba, “Adam: A method for stochastic optimization,” in *Proc. of ICLR*, Y. Bengio and Y. LeCun, Eds., 2015.

N. E. Toklu, T. Atkinson, V. Micka, P. Liskowski, and R. K. Srivastava, “Evotorch: Scalable evolutionary computation in python,” 2023.

A Broader Impact

This work focuses on certified defenses against adversarial attacks, which is a crucial component of trustworthy artificial intelligence. The potential harm of this work are as follows:

- Certified models can provide a fake sense of security when the models are used in conditions that permit adversarial attacks that are not considered in the training and certification process.
- Certification and certified training methods are computationally expensive, which will consume more energy if used for large-scale models and thus possibly harm the environment.

B PGPE Optimizes Smoothed Loss

B.1 Proofs

Lemma 3.1. *PGPE approximately minimizes the smoothed loss $L_\sigma(\theta)$ by sampling. In particular, the expectation of the PGPE update on θ is the true gradient of $L_\sigma(\theta)$, i.e., $\mathbb{E}\nabla_\theta \hat{L}_\sigma(\theta) = \nabla_\theta L_\sigma(\theta)$.*

Proof. This follows from the design principle of PGPE. For more details, see Sehnke et al. (2010) Sec. 2.1, Eqs. (1-10). \square

Corollary 3.2. *The loss surface under GLS is continuous, infinitely differentiable for any reasonably growing loss function $L(\theta)$.*

We further formalize the proof of this Corollary in the following Lemma.

Lemma B.1. *For any reasonably growing loss function $L(\theta)$ such that $|L(\theta)| \exp(-\theta^{2-\delta}) = O(1)$ for some $0 < \delta < 2$, let its Gaussian smoothing be $L_\sigma(\theta) = \mathbb{E}_{\epsilon \sim \mathcal{N}(0, \sigma^2)} L(\theta + \epsilon)$ for some $\sigma > 0$. Then $L_\sigma(\theta)$ is continuous and infinitely differentiable.*

Proof. $L_\sigma(\theta)$ exists due to the growth bound on $L(\theta)$. Further,

$$\begin{aligned} \frac{L_\sigma(\theta + \Delta\theta) - L_\sigma(\theta)}{\Delta\theta} &= \frac{1}{\Delta\theta} [\mathbb{E}_{\epsilon_1 \sim \mathcal{N}(\Delta\theta, \sigma^2)} L(\theta + \epsilon_1) - \mathbb{E}_{\epsilon_2 \sim \mathcal{N}(0, \sigma^2)} L(\theta + \epsilon_2)] \\ &= \int_{-\infty}^{\infty} \frac{1}{\Delta\theta} [P_{\epsilon_1}(x) - P_{\epsilon_2}(x)] L(\theta + x) dx \\ &= \int_{-\infty}^{\infty} \nabla_x \left[\frac{1}{\sqrt{2\pi\sigma^2}} \exp\left(-\frac{x^2}{2\sigma^2}\right) \right] L(\theta + x) dx \\ &= - \int_{-\infty}^{\infty} P_{\mathcal{N}(0, \sigma^2)}(x) L(\theta + x) \cdot \frac{x}{\sigma^2} dx. \end{aligned}$$

Since $|L(x)| \exp(-x^{2-\delta}) = O(1)$, the above integral is finite, thus $L_\sigma(\theta)$ has first-order derivative and is continuous.

Further, by setting $t = \theta + x$, we can rewrite the above integral as

$$\begin{aligned} L'_\sigma(\theta) &= - \int_{-\infty}^{\infty} P_{\mathcal{N}(0, \sigma^2)}(x) L(\theta + x) \cdot \frac{x}{\sigma^2} dx \\ &= - \int_{-\infty}^{\infty} P_{\mathcal{N}(\theta, \sigma^2)}(t - \theta) L(t) \cdot \frac{t - \theta}{\sigma^2} dt, \end{aligned}$$

thus

$$\begin{aligned} \frac{L'_\sigma(\theta + \Delta\theta) - L'_\sigma(\theta)}{\Delta\theta} &= - \int_{-\infty}^{\infty} \nabla_\theta \left[P_{\mathcal{N}(\theta, \sigma^2)}(t - \theta) \cdot \frac{t - \theta}{\sigma^2} \right] L(t) dt \\ &= - \int_{-\infty}^{\infty} P_{\mathcal{N}(0, \sigma^2)}(x) L(\theta + x) \cdot \frac{x^2 - \sigma^2}{\sigma^4} dx, \end{aligned}$$

which converges due to the growth bound on $L(\theta)$, thus $L_\sigma(\theta)$ has second-order derivative and is twice continuously differentiable. Similarly, we can show that $L_\sigma(\theta)$ has higher-order derivatives and thus infinitely differentiable. \square

Corollary 3.3. *The loss surface under GLS is β_1 -smooth for any reasonably growing β_2 -smooth loss function $L(\theta)$. The bounding constant β_1 of the GLS loss gradient is also less than or equal to the bounding constant β_2 of the original loss gradient.*

Proof. We cite this result from Starnes et al. (2023) Sec. 2 Lemma 2.5. \square

Corollary B.2. *The loss surface of PGPE is continuous, infinitely differentiable and more smooth than $L(\theta)$ for any reasonably growing loss function $L(\theta)$.*

Proof. This follows from Lemma B.1 and Lemma 3.1. \square

B.2 Alignment of Local and Global Minima under Gaussian Loss Smoothing

Without loss of generality, we consider a quantized function $f(x) = \sum_{i=0}^n a_i I(x \in [b_i, b_{i+1}])$, where I is the threshold function and $-\infty = b_0 \leq b_1 \leq \dots \leq b_n \leq b_{n+1} = +\infty$. The global minimum of this function is $\min_i a_i$, achieved by $x \in [b_{i^*}, b_{i^*+1}]$ where $i^* \in \arg \min_i a_i$. Now, the derivative of its Gaussian smoothed loss is $f'_\sigma(x) = \frac{1}{\sigma} \sum_{i=1}^n (a_i - a_{i-1}) p\left(\frac{b_i - x}{\sigma}\right)$, where p is the p.d.f. of the standard normal distribution. One may immediately find that the minimum of the smoothed loss is scale-invariant: the minimum of $f_{c\sigma}(cx)$ with b_i scaled by c is the same as the minimum of $f_\sigma(x)$. Therefore, if we increase σ to smoothen a fixed function, shallower minima with smaller widths will be smoothed out one by one. Taking σ to ∞ , we find that the derivative converges to zero, making the smoothed loss a constant function.

We use the same quantized function to study the effect smoothing has on the alignment of minimum points. As observed before, when we take σ to ∞ , the derivative on the whole domain converges to zero, so every point becomes a minimum, therefore we fail to get a proper alignment. On the other hand, by taking σ to zero, the factor $p\left(\frac{b_i - x}{\sigma}\right)$ becomes a Dirac delta function $\delta(x = b_i)$, thus every point except the boundary points becomes a local minimum, and we get the alignment of global minima. Based on these intuitions, one can pick a σ such that narrow local minima get smoothed out, and wide local minima are left close to their original locations, thus the optimization process can be guided towards the global minimum.

B.3 Properties of Randomized Gradient Smoothing

Discontinuity Considering again the quantized function as defined in App. B.2, we observe that the derivative of the original function is zero almost everywhere, so the smoothed gradient estimated by RGS will also be zero. This means that RGS is incapable of finding the minimum of the discontinuous functions in general. However, in practice we rarely work with quantized loss functions we used for the analysis; instead, we can model the discontinuous loss function as $h(x) = f(x) + g(x)$, where $f(x)$ is discontinuous like the quantized function and $g(x)$ is continuous. In this case, the derivative of h is equal to the derivative of g almost everywhere, and thus the RGS algorithm will converge to the same locations when optimizing h as when optimizing g . If the minima of g and h are sufficiently aligned, we can expect RGS to find a good minimum of h .

Higher Dimensions In higher dimensions, however, the behavior of RGS becomes unpredictable, as not every discontinuous function h can be decomposed into a continuous function g and a quantized function f (e.g. $h(x_1, x_2) = x_1 \cdot \text{sign}(x_2)$ consists of two plane sections separated by a discontinuity along the x_1 -axis). In this case, the equivalent loss landscape that the RGS algorithm is optimizing is strongly dependent on the optimization path and the starting point and therefore cannot be defined.

C Ablation Studies

C.1 Population Size

While PGPE recovers Gaussian Loss Smoothing in expectation, the quality of the gradient approximation depends strongly on the population size n_{ps} . In particular, a small population size n_{ps} induces a high-variance estimate of the true smoothed loss, leading to noisy gradient estimates and thus slow learning or even stability issues. We illustrate this in Figure 6 where we show the loss surface along the gradient direction for different population sizes. We observe that for small population sizes the loss surface is indeed very noisy, only becoming visually smooth at $n_{ps} = 512$. Additionally, PGPE computes a gradient approximation in an $\frac{n_{ps}}{2}$ -dimensional subspace, thus further increasing gradient variance if n_{ps} is (too) small compared to the number of network parameters.

To assess the effect this has on the performance of PGPE training, we train the same CNN3 on MNIST using population sizes between 64 and 1024, presenting results in Table 3. We observe that performance does indeed improve significantly with increasing population sizes (note the relative performance compared to initialization). This becomes even more pronounced when considering the training dynamics (see Figure 7). Unfortunately, the computational cost of PGPE is significant and scales linearly in the population size. We thus choose $n_{ps} = 256$ for all of our main experiments, as this already leads to training times in excess of 3 weeks on 8 V100s for some experiments.

Train Dynamics when varying population size In Figure 7 we present the evolution of the Training Loss during training with different values for popsize n_{ps} . We observe significantly slower training as we decrease n_{ps} , confirming the theoretical prediction that using lower popsize decreases the quality of gradient estimations due to increased variance in the loss-sampling process.

Table 3: Effect of the population size n_{ps} on accuracy and training time with PGPE + DEEPPOLY training on CNN3.

Popsize	Nat. [%]	Cert. [%]	GPU h
Init	97.14	94.02	-
64	97.22	94.07	88
128	97.22	94.13	160
256	97.30	94.19	304
512	97.27	94.22	596
1024	97.43	94.50	1192

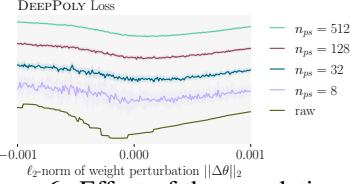


Figure 6: Effect of the population size n_{ps} on the smoothness of the induced loss surface in PGPE. Note that the 5 plots have been spaced by artificially adding offsets on the y-axis. This should not be regarded as a quantitative plot ordering the magnitude of the loss, but rather as a qualitative comparison of the smoothness induced by sampling with different population sizes.

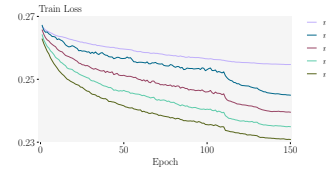


Figure 7: Evolution of Train Loss during training with different values for popsize n_{ps} . Note that for $n_{ps} = 64$ we trained with a lower learning rate because the value used in the other settings would make training unstable.

C.2 Standard Deviation

The standard deviation σ used for Gaussian Loss Smoothing has a significant impact on the resulting loss surface as we illustrated in Figure 5 and discussed in §3. If σ is chosen too small, the loss surface will still exhibit high sensitivity and gradients will only be meaningful very locally as discontinuities are barely smoothed. On the other hand, if σ is chosen too large, the loss surface will become very flat and uninformative, preventing us from finding good solutions.

When estimating the smoothed loss in PGPE via sampling at moderate population sizes n_{ps} , the standard deviation σ_{PGPE} additionally affects the variance of the loss and thus gradient estimate. We illustrate this in Figure 8, where we not only see the increasing large-scale smoothing effect discussed above but also an increasing level of small-scale noise induced by a large σ_{PGPE} relative to the chosen population sizes n_{ps} .

To assess the effect this practically has on PGPE training, we train for 50 epochs with different standard deviations σ_{PGPE} and present the results in Figure 9. As expected, we clearly observe that

both too small and too large standard deviations lead to poor performance. However, and perhaps surprisingly, we find that training performance is relatively insensitive to the exact standard deviation as long as we are in the right order of magnitude between 10^{-3} and 10^{-2} .

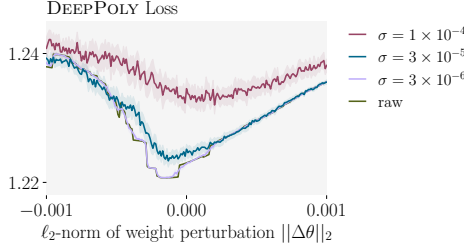


Figure 8: Effect of the standard deviation σ_{PGPE} on the induced loss surface in PGPE at a small population sizes of $n_{ps} = 32$.

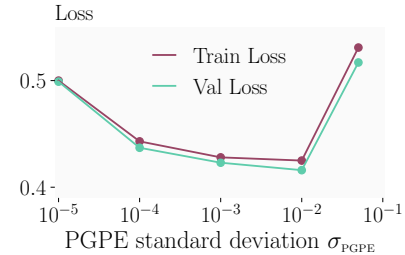


Figure 9: Train and Validation Losses after 50 epochs of training for different values of σ_{PGPE} .

D Additional Experimental Data

We provide additional experimental data for training CNN5 networks using DEEPOLY + RGS in Table 4. We observe that while DEEPOLY + RGS manages to obtain similar natural accuracies with gradient-based IBP, the certified accuracies are significantly lower. This is likely because to gain certifiability for the large epsilon settings the networks require a stronger regularisation than the DEEPOLY relaxation can provide.

Table 4: Accuracies of a CNN5 depending on training method.

Dataset	ϵ_∞	Method	Nat	Cert	Adv
MNIST	0.3	IBP	94.95	87.71	87.80
		SABR	97.78	88.26	89.33
		DEEPOLY-RGS	95.78	87.04	87.17
CIFAR-10	8/255	IBP	41.05	29.12	29.14
		SABR	43.30	29.50	29.55
		DEEPOLY-RGS	40.10	25.25	25.93

E Additional Training Details

E.1 Standard Certified Training

We train with the Adam optimizer (Kingma and Ba, 2015) with a starting learning rate of 5×10^{-4} for 70 epochs on MNIST and 160 epochs on CIFAR-10. We use the first 20 epochs on MNIST and 80 epochs on CIFAR-10 for ϵ -annealing and we decay the learning rate by a factor of 0.2 after epochs 50 and 60 for MNIST and respectively 120 and 140 for CIFAR-10.

E.2 PGPE Training

We use a training schedule of 150 epochs, with a batch size of 512 for MNIST and 128 for CIFAR-10. We train with a starting learning rate of 0.0003 and we decay it twice by a factor of 0.4 after the 110th and 130th epoch. We use the first 50 epochs for ϵ -annealing only when training with the large value of ϵ for each dataset (MNIST $\epsilon = 0.3$ and CIFAR-10 $\epsilon = 8/255$).

E.3 RGS Training

We use a training schedule of 60 epochs, with a batch size of 256 for MNIST and 80 epochs with batch size 128 for CIFAR-10. For the large ϵ setting of each dataset we add 20 extra epochs for ϵ -annealing at the beginning of training. We train with a starting learning rate of 0.0005 and we decay it twice by a factor of 0.4 for the last 2×10 epochs.

E.4 Architectures

In Table 5 we present the two network architectures used for all our experiments.

Table 5: Network architectures of the convolutional networks for CIFAR-10 and MNIST. All layers listed below are followed by a ReLU activation layer. The output layer is omitted. ‘CONV $c \times h \times w / s/p$ ’ corresponds to a 2D convolution with c output channels, an $h \times w$ kernel size, a stride of s in both dimensions, and an all-around zero padding of p .

CNN3	CNN5
CONV 8 $5 \times 5 / 2 / 2$	CONV 16 $5 \times 5 / 2 / 2$
CONV 8 $4 \times 4 / 2 / 1$	CONV 16 $4 \times 4 / 2 / 1$
	CONV 32 $4 \times 4 / 2 / 1$
	FC 512

E.5 Dataset and Augmentation

We use the MNIST (LeCun et al., 2010) and CIFAR-10 (Krizhevsky et al., 2009) datasets, all of which are freely available with no license specified.

The data preprocessing mostly follows Müller et al. (2023). For MNIST, we do not apply any preprocessing. For CIFAR-10, we normalize with the dataset mean and standard deviation (after calculating perturbation size) and augment with random horizontal flips. In addition, we apply random cropping to 32×32 after applying a 2 pixel padding at every margin for CIFAR-10.

E.6 Training costs (Time and Resources)

In Table 6 we present a detailed analysis of the training costs of the PGPE and RGS methods for all of our experimental settings (Note that the cost of DEEPPOLY-PGPE for CNN5 was estimated based on training for only 1 epoch).

Table 6: Training costs and workload distribution across GPUs / actors for each train setting.

Datset	Arch.	Relaxation	GPUs	Num. Actors	Time/epoch (min)	GPU-h/epoch
MNIST	CNN3	IBP	2 x L4	4	2.8	0.09
		SABR	2 x L4	4	7.6	0.25
		STAPS	2 x L4	4	17	0.57
		CROWN-IBP	2 x L4	4	8.5	0.28
		HBOX	8 x L4	8	31	4.13
		DEEPPOLY	8 x L4	8	27	3.60
	CNN5	DEEPPOLY (est.)	8 x L4	8	≈ 300	≈ 40
		DEEPPOLY (RGS)	8 x L4	8	7.5	1
CIFAR-10	CNN3	IBP	2 x L4	4	6.9	0.23
		SABR	4 x L4	8	14	0.93
		CROWN-IBP	4 x L4	8	8.5	0.57
		DEEPPOLY	8 x L4	8	42	5.6
	CNN5	DEEPPOLY (est.)	8 x L4	8	≈ 360	≈ 48
		DEEPPOLY (RGS)	8 x L4	8	16	2.2